Electronic structure and chemical-bonding mechanism of Cu_3N, Cu_3NPd, and related Cu(I) compounds

U. Hahn and W. Weber
Institute of Physics, University of Dortmund, D-44221 Dortmund, Germany
(Received 18 September 1995)

The electronic structure and the chemical-bonding mechanism of Cu_3N, Cu_3NPd and related Cu(I) compounds, such as Cu_2O, are studied on the basis of band-structure calculations, using both the linearized augmented plane wave and linear combination of atomic orbitals (LCAO) methods. In accordance with experimental observations, Cu_3N is found to be a semiconductor, while Cu_3NPd should exhibit a semimetallic conductivity. The chemical bonding is investigated using various methods, among them are the valence charge partitioning scheme of Bader and a basis set reduction technique built on the LCAO method. A partly ionic, partly covalent bonding is found. The admixture of the Cu $(4s, 4p)$ states to the Cu $3d$–N $2p$ bands resulted to be essential for the covalent bonding effect, since pure $3d$-$2p$ bands, with bonding and antibonding states fully occupied, do not lead to a covalent energy gain. This specific hybridization appears to be the origin of the twofold dumbbell like Cu(I) coordination observed in Cu_3N and other Cu(I) compounds. In Cu_3NPd, a covalent to metallic bonding between the Cu_3N host crystal and the interstitial Pd atoms is found, which is mainly caused by Pd $5s$ and $5p$ states hybridizing to Cu $3d$ states.

I. INTRODUCTION

The Cu(I) compound Cu_3N of anti-ReO_3 structure exhibits a remarkable structural feature: the Cu(I) ions form collinear bonds with two nearest neighbor anions.[1,2] Other Cu(I) compounds showing the same structural element are Cu_2O (Ref. 1), the delafossite compound $CuTaN_2$ (Ref. 3) and the cuprate $YBa_2Cu_3O_6$ (Ref. 4). It is possible to dope Pd into Cu_3N; both weakly doped $Cu_3NPd_{0.02}$ and stoichiometric Cu_3NPd are reported.[5] While pure Cu_3N is a semiconductor, the Pd doped nitrides show metallic behavior. In this paper, we present energy band calculations for Cu_3N and Cu_3NPd, using density functional theory. The main goal of our study is to investigate the chemical bonding in these materials, in particular, the nature of the Cu(I) collinear bonds.

The paper is organized as follows: In Sec. II, we survey the experimental situation concerning these materials. Then we present our band-structure calculations on Cu_3N and Cu_3NPd (Sec. III) and discuss the chemical bonding of these materials (Sec. IV). Conclusions are given in Sec. V.

II. EXPERIMENTAL SITUATION

The first synthesis of Cu_3N was achieved in 1939 by Juza and Hahn, who obtained polycrystalline powderlike material.[6] Using a high pressure high temperature growth technique under ammoniak atmosphere, Zachwieja and Jacobs were able to produce small single crystals of ≈ 1 mm length.[2] Cu_3N is metastable; it decomposes at 740 K into Cu and N_2. By x-ray diffraction the crystal structure was found to be of the anti-ReO_3 type, with a simple cubic unit cell of lattice constant 3.817 Å (see Fig.1). Based on an atomic form factor analysis, Zachwieja and Jacobs exclude the presence of Cu^{1+} and, in particular, N^{3-} ions in this material, instead the data are more compatible with almost neutral Cu and N atoms. This result points to the importance of covalent bonding. Another, more general argument for strong covalency effects is that ionic bonding leads to rather closely packed compounds, while the twofold Cu coordination can only occur in rather open structures. This open crystal structure of the anti-ReO_3 lattice is suited for the interposition of other elements, so that ternary Cu nitrides can be formed. Zachwieja and Jacobs have successfully synthesized the compound Cu_3NPd_x, with x values $0.020 \leqslant x \leqslant 0.989$, using similar high pressure high temperature techniques, as used for Cu_3N (Ref. 5). Cu_3NPd_x is also metastable and, independent of the Pd content, has the same decomposition temperature as Cu_3N. This observation suggests that the basic electronic structure of Cu_3N is maintained under Pd doping. The fact that Cu_3NPd_x is metallic, while Cu_3N is a semiconductor, may indicate that the insertion of Pd atoms only causes modifications of some energy bands near the Fermi energy. Cu_3NPd_x crystallizes in the cubic perovskite structure with the same space group $Pm3m$. The lattice constant for $x \approx 1$ is 3.850 Å. The chemical bonding between the Pd atoms and the Cu_3N host crystal is not understandable assuming completely filled Cu $3d^{10}$ or Pd $4d^{10}$ shells. Such a d^{10}-d^{10} bond is discussed by several authors in the context of substances like $Rb_2Cu_5O_4$ or $KAgCO_3$.[7–9] It is argued that low lying d^9s^1 or d^9p^1 configurations are responsible for that bond.

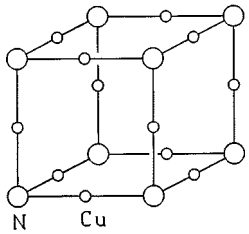

FIG. 1. Cu_3N unit cell.

Apart from Cu(I) compounds, there are several other compounds or molecules, where linearly coordinated cations (Ag^+, Au^+, Hg^{2+}) formally exhibit a closed d^{10} shell. Examples are Ag_2O, $[Ag(NH_3)_2]^+$, AuI, $[Au(CN)_2]^-$, HgS, and $[Hg(NH_3)_2]^{2+}$.[1,10] Since the excitation energy of all these cations from d^{10} into d^9s^1 configurations is rather low (2.7 eV in the case of a Cu^+ ion), Orgel has suggested in an early work that the hybridization of d $(3z^2)$ and s orbitals is responsible for the twofold coordination.[11]

Of the class of compounds with twofold metal atom coordination, Cu_2O is probably the most widely investigated material. Various energy band calculations have been performed[12–14] and the question of chemical bonding was discussed by Nagel and Marksteiner *et al.*[15,16] They agree that a purely ionic bonding mechanism with Cu $3d^{10}$ and O $2p^6$ closed shell ions is not adequate, but they do not state that covalency is an important part of the bond. Experimental support for a nonspherical Cu charge density is given by a large electric field gradient.[17,18] The theoretical value obtained by a linearized augmented plane wave (LAPW) calculation of Blaha and Schwarz agrees well with experiment.[19]

A further, well known compound of this class is the antiferromagnetic $YBa_2Cu_3O_6$,[4] where both Cu(I) and Cu(II) ions are present. Twofold Cu(I) coordination also occurs in the alloy $Li_{3-x}Cu_xN$ (Refs. 20 and 21). In the reference compound Li_3N, there exist two inequivalent Li sites, one of them is linearly coordinated with N. It is this site, where the Cu substitution takes place.

Another important structure is the delafossite type, with compounds of the formula ABX_2.[1,22] The X atoms form double layers with the B atoms sandwiched in between. The double layers are bonded via the twofold coordinated A atoms. Most of these substances are oxides (e.g., $CuAlO_2$, . . .), but one nitride is also known ($CuTaN_2$).[3]

There also exist Cu(I) compounds, where Cu(I) is higher coordinated. Examples are Cu_3P and Cu_2S, where the Cu ions do not form dumbbell like bonds, as in Cu_3N and Cu_2O (Refs. 23–25). In $CuAlS_2$ the Cu ions are fourfold coordinated.[1] One is lead to the assumption that the covalent bond strength between the Cu ions and the anions of row 3 of the Periodic Table is weaker than that with the anions of row 2. Nevertheless, CuCl of zinc blende structure[1] indicates that some residual covalent bonding is still present, otherwise one would expect that CuCl should form the typically ionic structures of NaCl or CsCl type.

III. BAND-STRUCTURE CALCULATIONS

A. Cu_3N

Our energy band calculations have been performed by using both the LAPW and the linear combination of atomic orbitals (LCAO) methods in order to combine the high accuracy of the former one, with the ability of the latter, to discuss the chemical bond with the help of the atomlike basis. We have employed the scalar relativistic full potential LAPW program package WIEN (Refs. 26 and 27) and the Gaussian orbitals based LCAO code of Appelbaum and Hamann.[28,29] Exchange and correlation were treated within the local density approximation (LDA), where we applied

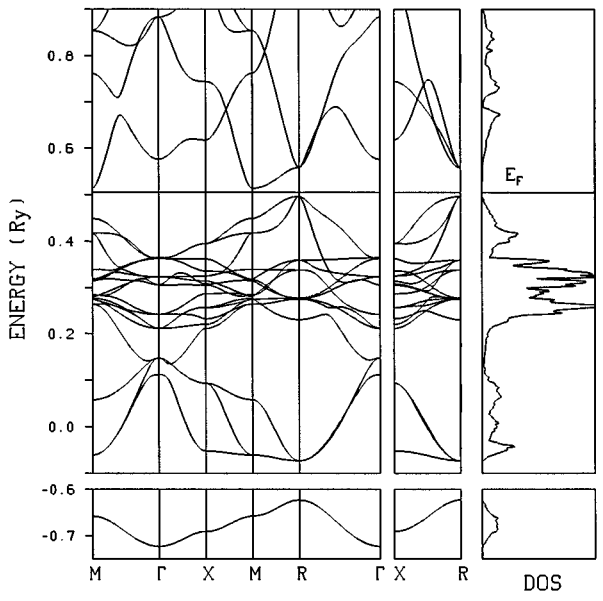

FIG. 2. LAPW energy bands and total density of states for Cu_3N.

the Hedin-Lundqvist parametrization[30] and, in the LCAO case, the Wigner interpolation formula.[31,32]

In the LAPW calculation, we have distinguished between the Cu $1s,2s,2p$ and N $1s$ inner shell electrons and the valence band electrons from the Cu $3d,4s,4p$ and N $2s,2p$ shell. The extended Cu $3s,3p$ states were handled separately as semicore bands. For the expansion of valence band and semicore wave functions, we have used bases of approximately 970 and 720 plane waves, respectively. In the muffin tin spheres, the l expansion of the wave functions was carried out up to $l_{max}=12$, whereas $l_{max}=6$ was chosen for the charge density and potential expansion. A mesh of 20 equally distributed k points was used for the Brillouin zone integration in its irreducible wedge.

Because of its smaller basis set the LCAO method is a more economic way to solve the Kohn-Sham equations than the LAPW scheme. In our calculations, we have considered the atomic Cu $3d,4s,4p,4d$ and N $2s,2p,3s,3p,3d$ orbitals for the valence band wave function expansion. In contrast to the LAPW calculations, where the core states were recalculated during the self-consistency cycle, the frozen core approximation was used for the Cu $1s,2s,2p,3s,3p$ and N $1s$ states. The radial parts of the atomic wave functions were presented as sums of up to 13 Gaussian functions, the exponential coefficients of which form a geometrical series. Crystal charge density and potential were also expanded in a set of Gaussian orbitals, we used 24 and 19 orbitals centered at the Cu and N atomic places, as well as some Gaussian functions located at selected auxiliary interstitial sites of high symmetry. Like in the LAPW calculation, the Brillouin zone integration was carried out using wave functions at 20 k points in its irreducible wedge.

The LAPW energy bands are shown in Fig. 2, also given there is the total density of states. The LCAO energy bands are very similar to the LAPW bands. An analysis of the eigenvectors allows us to extract information about the

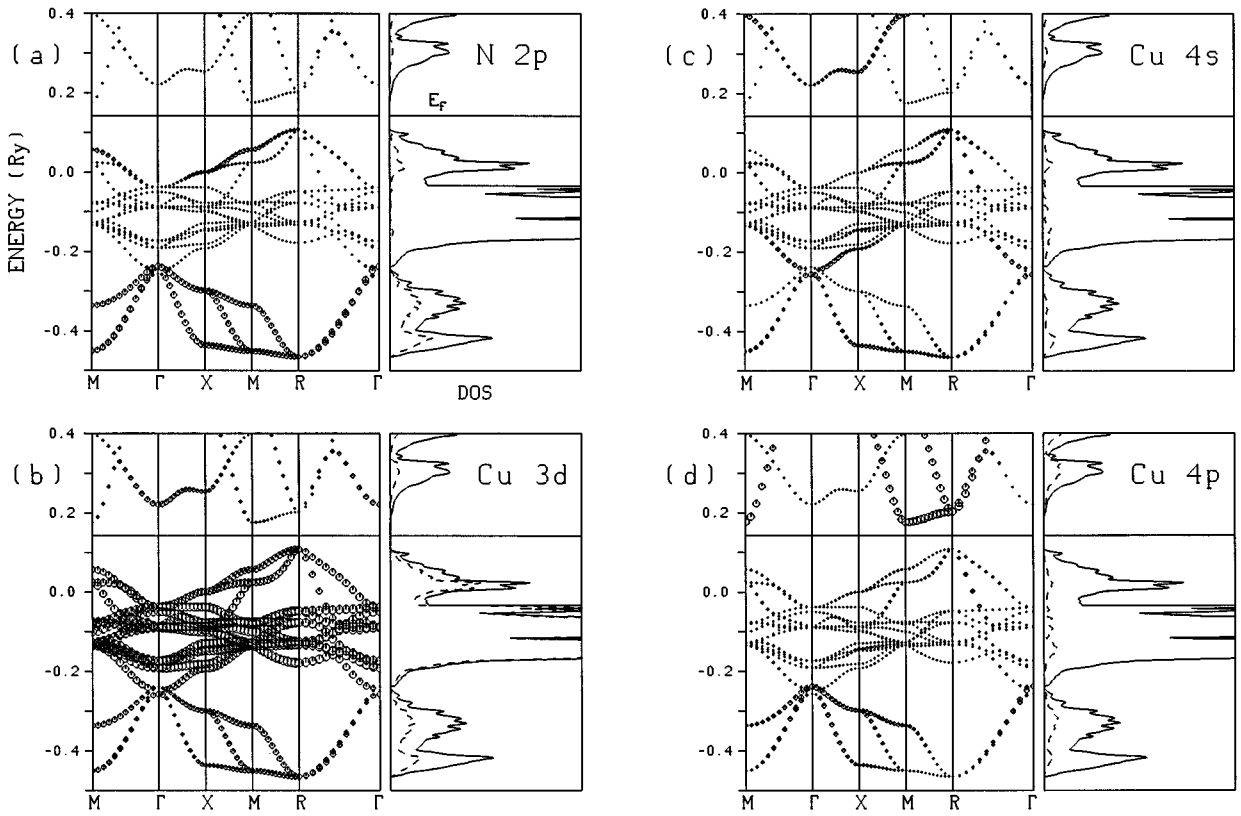

FIG. 3. LCAO energy bands, total (full line) and partial density of states (dashed line) for Cu_3N: (a) N $2p$, (b) Cu $3d$, (c) Cu $4s$, and (d) Cu $4p$. Symbol size indicates the strength of orbital character of the bands.

orbital character of the bands. The main results of this analysis are displayed in Figs. 3(a)–(d).

The calculations confirm that Cu_3N is a semiconductor. From the highly accurate LAPW calculation, we obtained the value of 0.23 eV for the energy gap, while the value of the less accurate LCAO method is found to be 0.9 eV. In view of the well known gap problem of the LDA, we expect the experimental gap to be of the order 0.5 eV.[33]

The energy bands of Cu_3N can be divided in three parts: a low lying N $2s$ band at -0.7 Ry, a broad valence band manifold of 0.6 Ry width, and the conduction bands. The group of the valence bands consists of three bonding and antibonding Cu $3d$–N $2p$ bands, which are separeted by 12 nonbonding bands. A decomposition of the Cu $3d$ partial density of states into contributions of $(3z^2)$, $(yz)/(zx)$ and $(xy)/(x^2-y^2)$ orbitals shows that the $(xy)/(x^2-y^2)$ states, which are oriented perpendicular to the N-Cu-N axis (i.e., the z axis), have negligible admixture to the bonding and antibonding bands (Fig. 4). A similar behavior was found by Marksteiner *et al.*, in the related compound Cu_2O.[16]

It should be noted that the bonding and antibonding bands are arranged asymmetrically around the nonbonding center and that the bandwidth of the antibonding states is considerably smaller than that of the bonding states. It will be shown below that this feature is strongly related to the covalent bonding between Cu and N, where the Cu $4s$ and $4p$ orbitals play an important role.

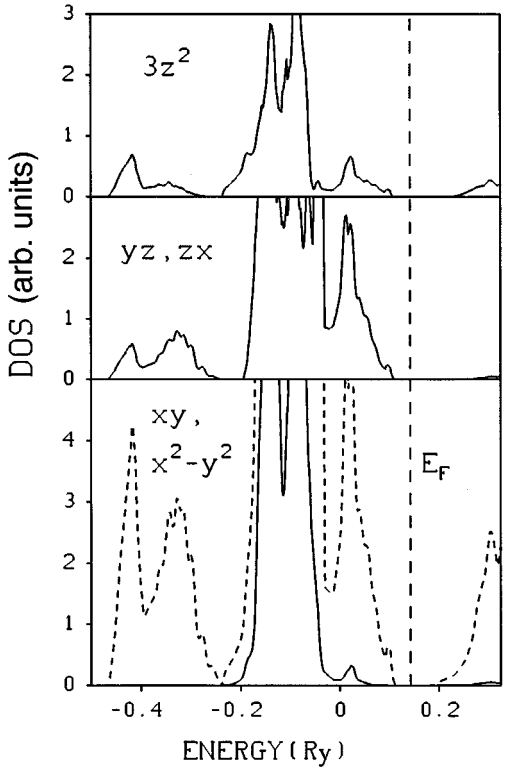

FIG. 4. Partial densities of states for the Cu $3d$ orbitals in Cu_3N. The N-Cu-N axis is chosen as z axis for the orbital projections. In the lowest panel, the total density of states is indicated by a dashed line.

B. Cu_3NPd

Since Cu_3N is the parent compound of Cu_3NPd, we have used very similar computational parameters in the band-

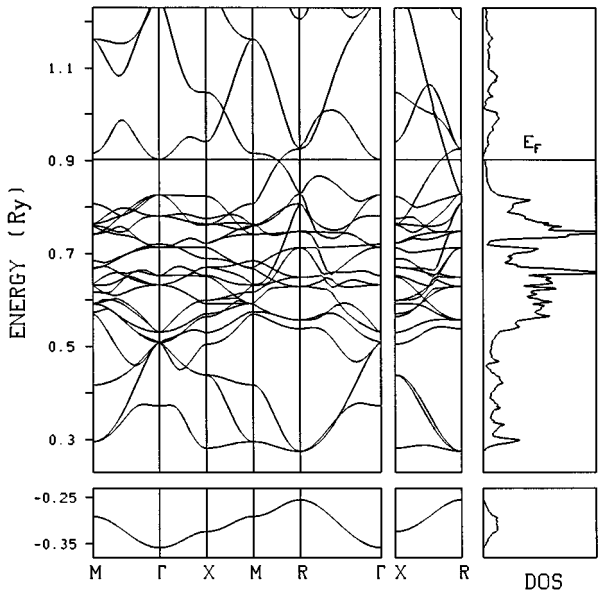

FIG. 5. LAPW energy bands and total density of states for Cu_3NPd.

structure calculations of both systems. Apart from some shifts of the Cu and N l-expansion energy parameters, the major modification of the LAPW calculation is to consider the Pd $4s,p$ orbitals as semicore bands. The Pd $4d$,5s states were treated as valence bands. In the LCAO calculation, we had to change the charge and potential expansion and we utilized the valence band basis set of Cu_3N, which was completed by the Pd $4d$,5s,p,d states. Due to the larger number of matrix elements, we have reduced the number of k points used for the Brillouin zone integration in the LCAO scheme, from 20 to 10. Again, as in the case of the Cu_3N compound, the agreement between the LAPW and the LCAO calculation is good.

The energy bands of Cu_3NPd are displayed in Fig. 5. By the comparison with Fig. 2, it is obvious that the Cu_3N–band structure is only slightly affected by Pd doping in its lower parts (i.e., N 2s bands, N-Cu bonding states). However, the antibonding bands near the Fermi energy interact with the Pd 4d states. In addition, the Cu 3d nonbonding states hybridize with the Pd 4d orbitals, as indicated by the partial density of states [Figs. 6(a)–(c)]. The most interesting point of the Cu_3NPd bandstructure is certainly the intersection of bands at the Fermi energy between the symmetry points M and R and between R and X, leading to a semimetallic, rather than metallic behavior of the system. In contrast to the band crossing between R and X, the intersection between M and R is not removed by spin-orbit coupling. If the energy of the Γ-point conduction band lies slightly above the crossing point, a semimetallic behavior with vanishingly small density of states at Fermi energy would exist. If the Γ point energy lies slightly below the crossing point energy, the Fermi surface would consist of an electron pocket around Γ and a hole pocket around the crossing point. We believe that the uncertainties of the LDA results are larger than the observed energy difference, so that we feel unable to decide which case is more probable.

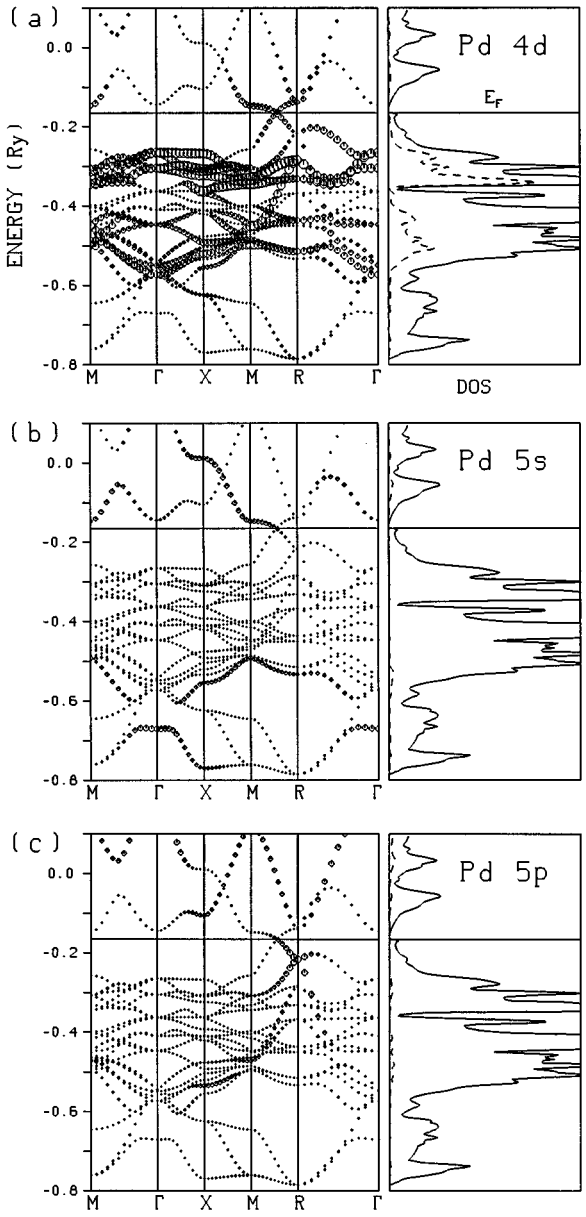

FIG. 6. LCAO energy bands, total (full line) and partial density of states (dashed line) for Cu_3NPd: (a) Pd 4d, (b) Pd 5s, and (c) Pd 5p. The size of the symbols indicates the strength of orbital character of the bands.

IV. CHEMICAL BONDING

As mentioned in Sec. II, there are strong indications that a purely ionic model is not adequate to describe the chemical bonding in the Cu(I) compounds. Instead one has to suppose a combination of ionic and covalent bonding mechanisms. The two contributions are now analyzed. The ionic bond strength is investigated by considering the spatial distribution of the charge density in the Cu_3NPd_x system and by determining the charge transfer between the constituents, as a measure of ionicity. Large deviations from a simple $Cu^{1+}N^{3-}$ picture are found.

The covalent bonding is analyzed by several techniques, which make use of the atomlike basis set within the LCAO scheme. We achieve an understanding of the covalent bond

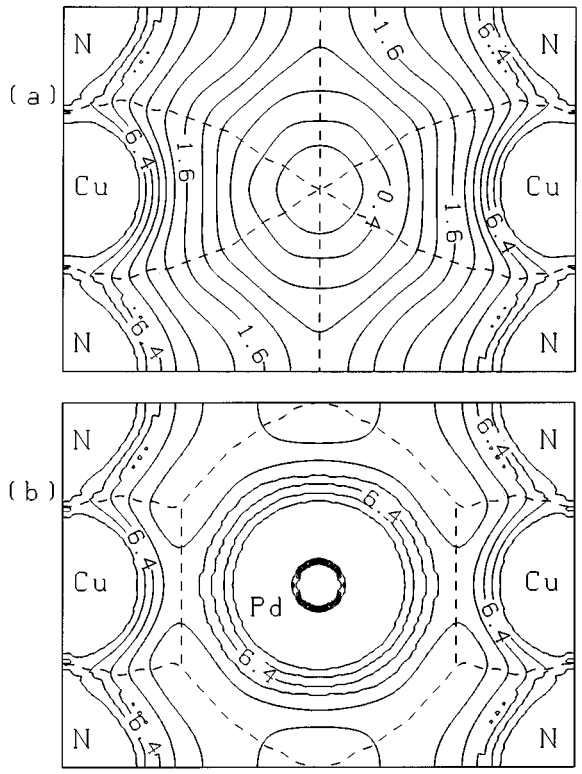

FIG. 7. Contour map of the LAPW valence band electron density for (a) Cu_3N and (b) Cu_3NPd. The values are given in units of $0.01e/a_B^3$. Consecutive lines differ by a factor 1.414. The partition of the unit cell in accordance with Bader's scheme is indicated by dashed lines.

as a hybridization effect of the Cu $4s,p$ orbitals, with the bonding and antibonding N $2p$–Cu $3d$ bands.

By performing energy band calculations on the related compound Cu_2O in its real structure, as well as in the antifluorite structure, of the alkali oxides, it could be shown that covalency is responsible for the twofold linear coordination of Cu(I) in numerous compounds.

Finally, the bonding mechanism of Pd in the Cu_3N host crystal is analyzed.

A. Ionic bonding

The ionic bonding mechanism can easily be understood by the electrostatic attraction of ions with different charges. Assuming a nearly spherical charge distribution of the ions, which is justified in the case of compounds like the alkali halides, the bond energy of the crystal is calculated in accordance with Madelung's concept. Substances where the ions show strong deviations from spherical charge symmetry or where the total charge of the ions is unknown, cannot be handled by this scheme. As we will see below, the Cu compounds described here consist of N anions and Cu cations with open $2p$ and $3d$ shells, as well as partially occupied Cu $4s,p$ states. Since it is not easy to generalize Madelung's concept for open shell systems, we restricted ourselves to determine the total charge of the constituents, which can be regarded as a qualitative measure of the ionic bond strength. A very natural way of dividing the charge distribution of a molecule or crystal and a definition of total atomic charge was introduced by Bader and Bedall.[34] This method is based on the analysis of the gradient of the charge density $\rho(\vec{r})$. The charge $dQ=\rho(\vec{r}_0)dV$ contained in a certain volume element dV is attributed to the atom, which is the destination of the gradient path starting from $\vec{r}_0$. Such a procedure leads to a partition of the system, and the boundary surfaces of the various parts are given by the zero flux condition,

$$\vec{n}(\vec{r})\,\mathrm{grad}\rho(\vec{r})=0, \tag{1}$$

with $\vec{n}(\vec{r})$ being the normal vector of the surface. This analysis was applied to the Cu_3N and Cu_3NPd charge densities and we obtain a division, as shown in Fig. 7. The integrated charges of each atom are listed in Table I. Good agreement between the LAPW and LCAO results is obtained. The values of the Cu and N charges are approximately $+0.5$ and -1.5, which clearly demonstrates that Cu_3N is not built of Cu^{1+} and N^{3-} ions. A considerable population of the Cu $4s,p$ states is present and indicates a covalent bonding mechanism.

In Cu_3NPd, one finds a small electron transfer from Cu and N to the Pd atoms, which are negatively charged. This effect may be explained either by a reduction of the Cu/N integration volumes or by covalency effects.

TABLE I. Integrated atomic charges, as obtained from Bader's method of charge partitioning, both for the LAPW and the LCAO valence band electron density.

		LAPW	LCAO
Cu_3N	Cu	+0.54	+0.47
	N	-1.62	-1.40
Cu_3NPd	Cu	+0.63	+0.52
	N	-1.46	-1.28
	Pd	-0.45	-0.26

B. Covalent bonding

In contrast to the ionic bond, the covalent bonding mechanism is a quantum effect, which cannot be understood in the context of classical physics. The central point is the interfer-

TABLE II. Occupation of the LCAO Löwdin states, for Cu_3N and Cu_3NPd. The values refer to a single atom and both spin directions.

	N			Cu				Pd			
	tot	$2s,p$	$3s,p,d$	tot	$3d$	$4s$	$4p,d$	tot	$4d$	$5s$	$5p,d$
Cu_3N	4.77	4.05	0.72	11.08	9.38	0.51	1.19				
Cu_3NPd	4.74	3.93	0.81	11.05	9.17	0.43	1.45	10.10	8.77	0.37	0.96

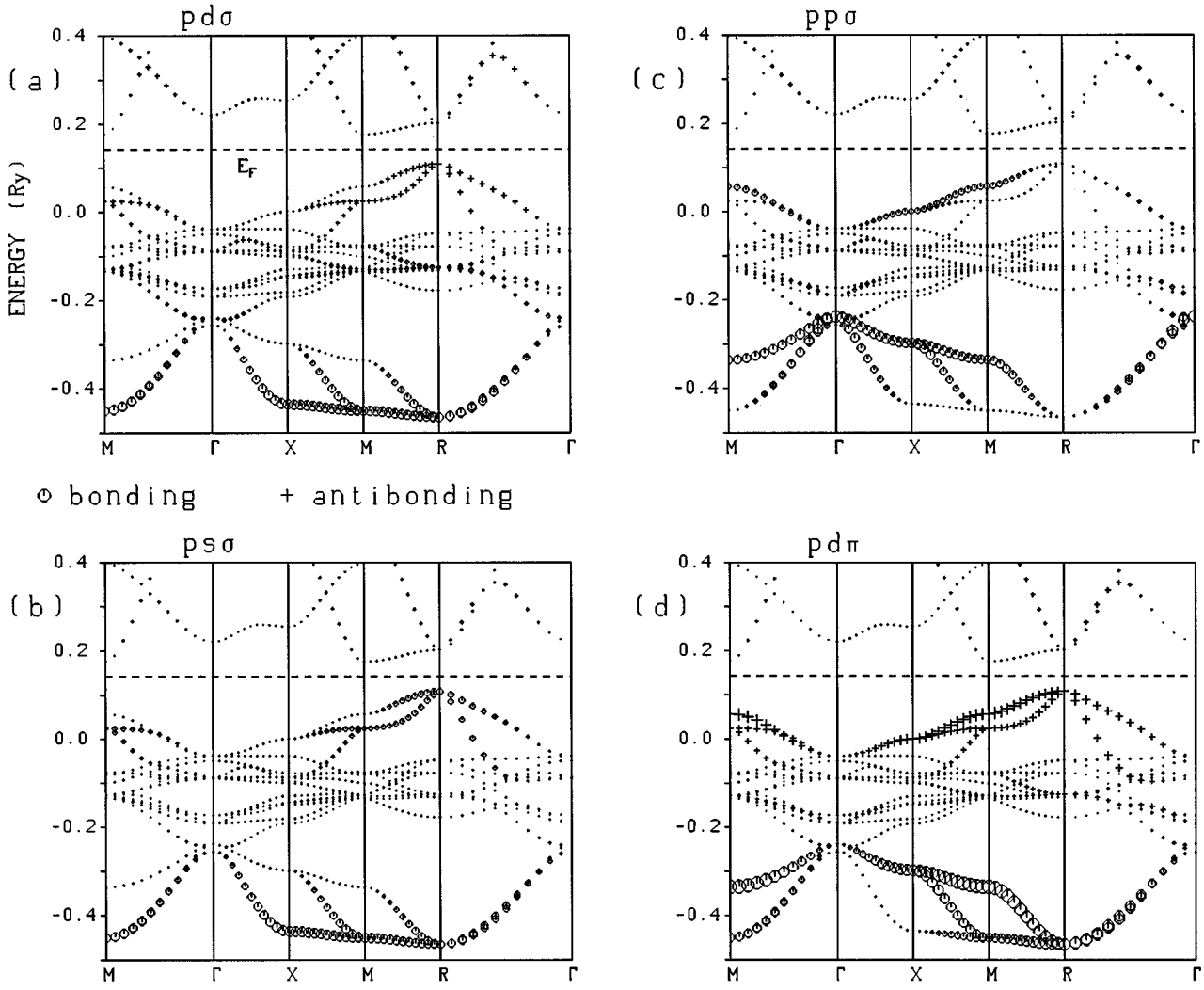

FIG. 8. Bonding analysis for the LCAO energy bands for Cu_3N. Symbol size indicates the strength of the bonding or antibonding character of the bands. The analysis comprises (a) N $2p$ Cu $3d$ $pd\sigma$, (b) $2p$ $4s$ $ps\sigma$, (c) $2p$ $4p$ $pp\sigma$, and (d) $2p$ $3d$ $pd\pi$ bonds.

ence of orbitals at neighboring atoms. Constructive interference leads to bonding states, while antibonding states are the result of destructive interference. When the resulting charge density is mainly situated along the bond (bond charge), the limit of purely covalent bonding is obtained, when the charge density is spread rather homogeneously over the whole unit cell, we have the limit of metallic bonding. There is no energy gain, i.e., no covalent bonding, if both bonding and antibonding states are fully occupied. One might think of such a situation in Cu_3N under the assumption of closed shell Cu and N ions, with $3d^{10}$ and $2p^6$ configurations. In order to discard this possibility and to understand the important role of the Cu $4s,p$ orbitals, we have employed a population analysis and two other methods, which we call ''projection technique'' and ''basis set reduction.'' Since the nonorthogonal atomic orbitals of the LCAO basis set do not allow a unique charge assignment, the results of the population analysis (Table II) refer to the respective Löwdin states.[35] A nearly half filled N $2s$ orbital and a slightly positive N ion require a careful interpretation of these data, the insufficiencies of which must be attributed to the large overlap of the extended Cu $4s,p,d$ states with the N orbitals. A rather large population of these Cu states is contrasted by a depletion of both the Cu $3d$ and even more of the N $2p$ orbitals. The formation of Cu $3d$ holes occurs especially in the $(3z^2)$ states, which are directed towards the N atoms, indicating a Cu-N bond.

A better understanding of the Cu-N bond can be obtained by a projection analysis, which investigates the interference process of neighboring atomic orbitals. In the case of the dominating N-Cu $pd\sigma$ bond, one can define bonding and antibonding reference states

$$|b\rangle := \frac{1}{\sqrt{2}}(|p_z\rangle + |3z^2\rangle), \tag{2}$$

$$|ab\rangle := \frac{1}{\sqrt{2}}(|p_z\rangle - |3z^2\rangle),$$

where $|p_z\rangle$ and $|3z^2\rangle$ are localized at the N and Cu sites and are assumed to be orthogonal. A projection $\lambda_{i\vec{k}} := |\langle b|i\vec{k}\rangle|^2 - |\langle ab|i\vec{k}\rangle|^2$ of these states onto a band wave function $|i\vec{k}\rangle$ is a measure of the bonding or antibonding

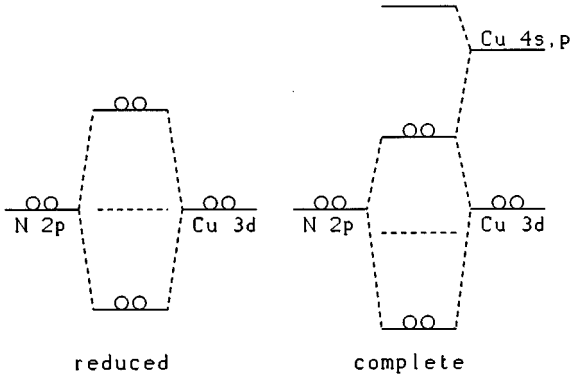

FIG. 9. Energy levels of a N-Cu three orbital model system, indicating the Cu $3d$-$4s$ to N $2p$ hybridization.

character. This analysis is applied on the N $2p$–Cu $3d$,$4s$,p bond and the results are plotted in Fig. 8. Bonding as well as antibonding phase relations are found in the case of the $pd\sigma$ and $pd\pi$ bond, whereas there is always a bonding phase relation between the N $2p$ and Cu $4s$,p states below Fermi energy.

A more direct indication of covalent bonding, other than by population and projection analysis, is obtained by the reduction of the LCAO basis set. It can be shown that the use of a limited LCAO basis consisting of N $2s$,p and Cu $3d$ states leads to significant changes in the band energies. The essential parts of this procedure can be understood by a three level toy model, the states of which are assumed to represent the nearly degenerate N $2p$, Cu $3d$ orbitals and the Cu $4s$ state of higher energy (Fig. 9). Hybridizing only the N $2p$, with the Cu $3d$ state, does not result in a covalent bond, since bonding and antibonding states are fully occupied and their center of gravity coincides with the N/Cu onsite energy. An additional coupling between the N $2p$ and Cu $4s$ orbitals (described by a transfer matrix element t) causes a lowering Δ of the center of gravity and leads to a bonding effect. By second order pertubation theory, Δ is calculated to be

$$\Delta = \frac{1}{2}(\Delta_{\text{bond}} + \Delta_{\text{antibond}})$$

$$= -\frac{t^2}{4}\left(\frac{1}{\varepsilon_{4s,p} - \varepsilon^0_{\text{bond}}} + \frac{1}{\varepsilon_{4s,p} - \varepsilon^0_{\text{bond}}}\right).$$

The larger shift of the antibonding state is caused by the smaller denominator. This simple model compares very well

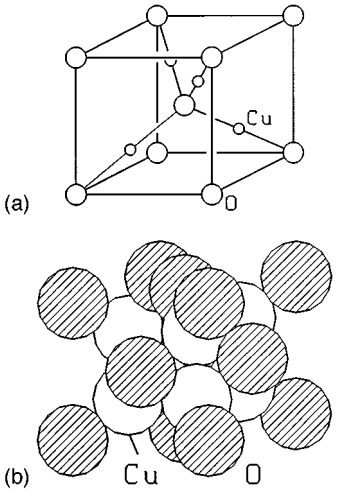

FIG. 11. (a) Cu_2O crystal structure and (b) antifluorite structure.

with the real LCAO band structure when we carry out a similar change of the basis set (Fig. 10). The full LCAO basis consists of N $2s$,p;$3s$,p,d and Cu $3d$;$4s$,p,d states whereas, in the reduced basis, the N $3s$,p,d and Cu $4s$,p,d orbitals are omitted. For better comparison, the same potential as in the full calculation was used for the restricted basis set calculation. The latter calculation yields energy bands with bonding and antibonding states arranged nearly symmetrically around the nonbonding Cu bands. On the other hand, the full basis set calculation produces the nonsymmetric shifts, as discussed in the toy model. The comparison with the projection analysis diagrams (Fig. 8) shows that the largest shifts occur in bands with $(2p-4s)\sigma$, rather than $(2p-4p)\sigma$ N-Cu hybridization. Obviously, the hybridization of the Cu $4s$ orbitals is more important than that of the Cu $4p$ states.

C. Linear Cu coordination

The common feature of the Cu(I) compounds discussed in this work is the linear coordination of Cu with anions. Copper oxide (Cu_2O) rather than the copper nitride seems to be the ideal system to study the competition between the ionic and covalent bonding mechanism: the real Cu_2O structure can be compared with the closely packed antifluorite structure, which alkali oxides form (Fig. 11).

The technical details of the LCAO band-structure calculations performed on Cu_2O are very similar to those of

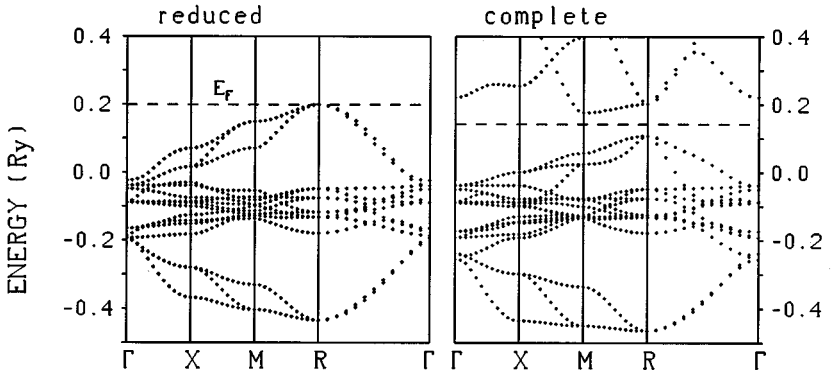

FIG. 10. LCAO band structure for Cu_3N calculated with reduced and full basis sets. For details see text.

TABLE III. Occupation of the LCAO Löwdin states for Cu_2O. The values are given for the real structure and the ficticious antifluorite structure at equilibrium lattice constant.

	Cu					O			
	tot	$3d$	$4s$	$4p$	$4d$	tot	$2s$	$2p$	$3s,p,d$
Real	11.10	9.36	0.53	0.69	0.52	5.81	1.18	3.98	0.65
Anti-CaF_2	10.98	9.29	0.31	0.66	0.72	6.08	1.36	3.84	0.88

Cu_3N. In order to avoid systematic errors in comparing both structures, charge and potential expansion were carried out without any auxiliary interstitial sites, the number and position of which would be different in the two cases. The energy bands of the real Cu_2O are in good agreement with the LAPW result of Marksteiner *et al.*[16] In contrast to Cu_3N, Cu_2O is a direct semiconductor. Total energy calculations of the ficticious Cu_2O, with antifluorite structure, yield a nearest neighbor separation, which is 15% larger than in the real system and a total energy per formula unit, which is 0.1 Ry larger. Also, metallic behavior is found.

Similarly to Cu_3N, the LCAO population analysis results in nearly neutral Cu atoms (Table III). On the other hand, the gradient analysis yields a Cu charge of approximately $+0.4$, both for the real and the ficticious structure. Like in Cu_3N, the formation of holes in the linearly coordinated Cu takes place predominantly in the $(3z^2)$ states. As a consequence, the Cu $4s$ occupation in the real structure is larger than in the antifluorite case.

For Cu_2O, we have investigated, in detail, the effects of basis set reduction. We have not only compared LCAO band structures calculated with full (Cu $3d;4s,p,d$; O $2s,p;3s,p,d$) and reduced basis set (Cu $3d$; O $2s,p$), but also employed partially reduced basis sets, where one of the higher lying Cu $4s,p,d$ or O $3s,p,d$ orbitals has been included. Going from a reduced to full basis set, a more pronounced gain of band energy is found for the real structure than for the antifluorite one (Table IV). When we study the changes from the reduced to partially reduced basis sets, we find the following results: In the case of the antifluorite structure, the largest gain is obtained when Cu $4p$ states are included, whereas in the real structure, the Cu $4s$ orbitals are more effective. It, thus, appears that the hybridization of $4s$ and $3d$ $(3z^2)$ orbitals cause the linear Cu coordination.

Note that for linearly coordinated Cu(I) the $4s$ and $3d$ $(3z^2)$ orbitals belong to the same representation. Then, a coupling of these orbitals through the crystal field is possible, also of course, the coupling through hopping to neighbor anion sites. The idea of Cu $3z^2$-$4s$ hybridization, as a mechanism for explaining the dumbbell like bond, was proposed by Orgel.[11] In contrast to the present work, covalency is not explicitly given as the mechanism which determines the structure.

TABLE IV. Gain in band energy for Cu_2O, using various LCAO basis sets, as compared to the minimum basis set (Cu $3d$; O $2s,p$). The values (in Ry per unit cell) are given for the real and the ficticious antifluorite structure. Partially reduced basis sets include the minimum basis and the orbital given in the table.

		Cu			O		
	Full basis	$4s$	$4p$	$4d$	$3s$	$3p$	$3d$
Real	0.72 Ry	0.35	0.22	0.11	0.07	0.23	0.04
Anti-CaF_2	0.59	0.29	0.31	0.16	0.05	0.28	0.09

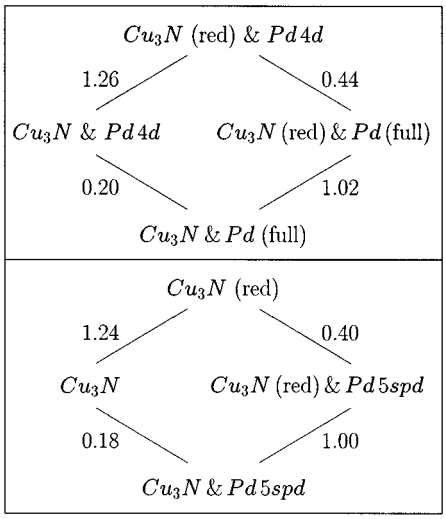

FIG. 12. Scheme indicating the gains in band energy (in Ry per unit cell), when going from reduced basis sets to the full basis. The various basis sets of the lower panel are omitting the Pd $4d$ states (see text for details).

This section is concluded with some comments on the role of the neighboring anion. As mentioned in the introduction, the dumbbell like bond occurs predominantly in compounds with anions from the 2nd row and not with those of row 3. We have performed additional LCAO band-structure calculations (not presented here) on Cu_2S in Cu_2O structure and on CuF/CuCl in zinc blende structure. It has been found that the effect of basis set reduction, as a measure of covalent bond strength, is more distinct in the case of the 2nd row anions. The larger Cu coordination number in compounds with 3rd row anions may therefore be attributed to the relatively larger influence of ionic bonding.

It is interesting to note that the different behavior of row 2 and row 3 atoms is also observed in elemental solids or molecules. Graphite is a more stable modification of carbon than the diamond structure, which is preferred by silicon. Oxygen and nitrogen form diatomic molecules, whereas sulfur and phosphorus exist as S_8 or P_4.

D. Pd bonding mechanism

In normal perovskite crystals like $BaTiO_3$, alkali or earth alkaline elements are placed on the position, which is occupied by Pd in Cu_3NPd. The bonding mechanism of these cations appears to be predominantly ionic. Although there is a minor ionic effect in the case of the slightly negatively charged Pd atom, a covalent bonding contribution seems to be more important. Like in the previous section, our investigations are based on population analysis, projection, and basis set reduction techniques. In Table II, the LCAO population analysis results of Cu_3N and Cu_3NPd are compared. One finds a certain charge transfer from Cu and N to Pd, the LCAO total negative charge (-0.10) of which is

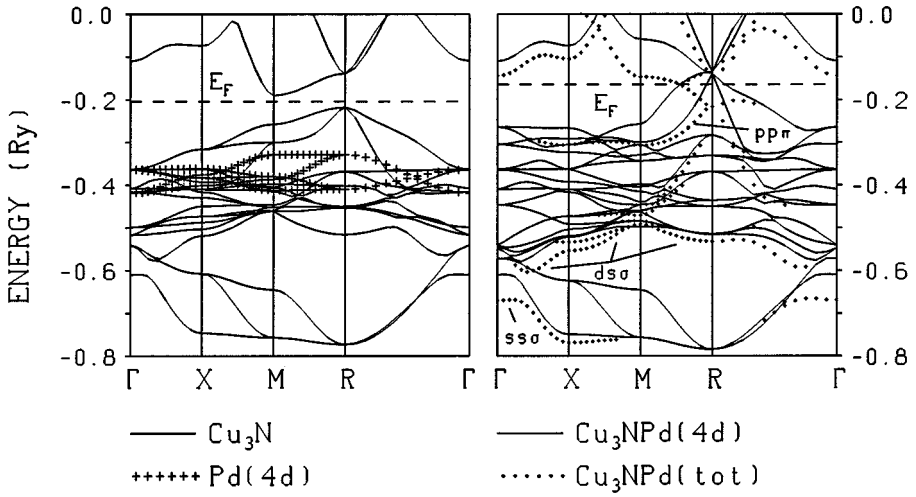

FIG. 13. Energy bands calculated with various basis sets, by using the full Cu_3NPd potential (see text). Left side: complete Cu_3N basis (case i) and isolated Pd orbitals (case ii). Right side: Partially reduced Cu_3NPd basis (case iii) and complete Cu_3NPd basis (case iv). For (case iv), only the most significant deviations are shown by dots. The predominant bonding character of these bands is also indicated.

smaller than that calculated with Bader's method (-0.45). The Pd atoms do not have a filled d^{10} shell, which can be regarded as an indication for a covalent or metallic Cu-Pd bond.

The projection technique has been applied on the Cu-Pd $dd\sigma$, $ds\sigma$, $ss\sigma$, and some other bonds (not shown here). Below the Fermi energy, bonding, and antibonding phase relations are found in the case of the $dd\sigma$ and $dd\pi$ bonds. However, a strong bonding phase relation is observed between the Cu/Pd d and the higher lying s,p states of the neighboring atoms.

It has been demonstrated above that there is no covalent bond in Cu_3N, if the Cu and N ions have $3d^{10}$ and $2p^6$ configurations. A similar behavior is expected for a closed shell $4d^{10}$ Pd atom, which is placed into a Cu_3N host crystal. A covalent Cu-Pd bond must, therefore, be caused by $4d$ holes and by an occupation of the higher lying Cu $4s,p,d$ and Pd $5s,p,d$ orbitals. Since these Cu states are also responsible for the Cu-N bond, one can attempt to single out their importance for the Cu-Pd bond by the following procedure. The restricted basis sets of Cu_3NPd (Cu $3d$; N $2s,p$; Pd $4d$) and of Cu_3N (Cu $3d$; N $2s,p$) are completed both step by step by the (Cu $4s,p,d$; N $3s,p,d$) and (Pd $5s,p,d$) orbitals. The resulting band energy gains are illustrated in Fig. 12. All energy band calculations have been carried out with the converged Cu_3NPd potential and the Fermi energy of the ''pseudo'' Cu_3N was determined by neglecting the ten $4d$ electrons of Pd. We find that the energy gains do not depend much on the presence of the Pd $4d$ orbitals. One can conclude that a bond between Cu $4s,p$ and Pd $4d$ states is of less importance and that the Cu $3d$–Pd $5s,p$ bonding is dominating. As the resulting charge density is not very much enhanced along the Cu-Pd direction, the bonding appears to be more metallic than covalent.

One can get further insight into the Pd bonding mechanism, by studying energy bands calculated by using four different basis sets (Fig. 13). Keeping the fully converged crystal potentials, we employed (i) the complete Cu_3N basis, (ii) the Pd $4d$ orbitals, (iii) a $Cu_3NPd(4d)$, and (iv) a complete Cu_3NPd basis set. (i) Results in energy bands which are in good agreement with the Cu_3N bands of Fig. 2. The bands of the isolated Pd $4d$ states (case ii) have less dispersion and they are positioned in the upper parts of the nonbonding Cu bands. They are shifted up by ≈ 0.1 Ry, if they are allowed to hybridize with the Cu_3N bands (case iii). When the Pd $5s,p,d$ states are also included (case iv), some specific bands are lowered, while the majority is only slightly affected. A comparison with the projection analysis indicates that Cu-Pd $ss\sigma$, $ds\sigma$, and $pp\pi$ bonding relations cause the largest shifts. Our analysis is compatible with the proposal of several authors (e.g., Refs. 7–9) that low lying s and p states are responsible for the d^{10}-d^{10} bond in numerous compounds.

V. CONCLUSIONS

We have carried out LAPW and LCAO energy band calculations on Cu_3N and Cu_3NPd, in order to study the electronic structure and bonding mechanism of these and related Cu(I) compounds. Cu_3N is confirmed to be a semiconductor, while Cu_3NPd should exhibit semimetallic behavior. The chemical bonding analysis of Cu_3N shows a combination of ionic and covalent bonding. By applying the Bader partitioning scheme, the ionic charges of Cu and N were calculated to be approximately $+0.5$ and -1.5 rather than $+1$ and -3.

We found that the LCAO method is a very effective tool for analyzing the covalent bonding contributions. We have used the population analysis, projection and basis set reduction techniques and have achieved an understanding of the covalent bond as a hybridization effect between the Cu $3d$–N $2p$ bands and the Cu $4s,p$ conduction bands. The dumbbell-like Cu bond has been analyzed in the case of cuprous oxide Cu_2O, by comparing its real structure with the ficticious antifluorite lattice, which is preferred by the alkali oxides. It has been found that the characteristics of the covalent bond are more pronounced in the real Cu_2O structure. The bonding between Pd and the Cu_3N host crystal, often called a ''d^{10}-d^{10}'' bond, is caused by a covalent to metallic bonding involving more the Pd $5s$ and $5p$ than the Cu $4s$ and $4p$ states.

ACKNOWLEDGMENTS

We would like to thank H. Jacobs, U. Zachwieja, and G. Vielsack for helpful discussions. This work was supported by the Deutsche Forschungsgemeinschaft (Graduiertenkolleg Festkörperspektroskopie).

[1] R.W.G. Wyckoff, *Crystal Structures*, 2nd ed. (Wiley, New York, 1963), Vols. 1 and 2.
[2] U. Zachwieja and H. Jacobs, J. Less-Common Met. **161**, 175 (1990).
[3] U. Zachwieja and H. Jacobs, Eur. J. Solid State Inorg. Chem. **28**, 1055 (1991).
[4] A. Santoro, S. Miraglia, S.A. Sunshine, D.W. Murphy, L.F. Schneemeyer, and J.V. Waszczak, Mater. Res. Bull. **22**, 1007 (1987).
[5] U. Zachwieja and H. Jacobs, J. Less-Common Met. **170**, 185 (1991).
[6] R. Juza and H. Hahn, Z. Anorg. Allg. Chem. **241**, 172 (1939).
[7] M. Jansen, Angew. Chem. **99**, 1136 (1987).
[8] P.K. Melrotra and R. Hoffmann, Inorg. Chem. **17**, 2187 (1978).
[9] K.M. Merz and R. Hoffmann, Inorg. Chem. **27**, 2120 (1988).
[10] C.E. Mortimer, *Chemistry* (Wadsworth Publishing, Belmont, 1986).
[11] L.E. Orgel, J. Chem. Soc. **1958**, 4186 (1958).
[12] J. P. Dahl and A.C. Switendick, J. Phys. Chem. Solids **27**, 931 (1966).
[13] L. Kleinman and K. Mednick, Phys. Rev. B **21**, 1549 (1980).
[14] J. Robertson, Phys. Rev. B **28**, 3378 (1983).
[15] S. Nagel, J. Phys. Chem. Solids **46**, 743 (1985).
[16] P. Marksteiner, P. Blaha, and K. Schwarz, Z. Phys. B **64**, 119 (1986).
[17] H. Krüger and U. Meyer-Berkhout, Z. Phys. **132**, 171 (1952).
[18] T. Kushida, G.B. Benedek, and N. Bloembergen, Phys. Rev. **104**, 1364 (1956).
[19] P. Blaha and K. Schwarz, Hyperfine Interact. **52**, 153 (1989).
[20] A. Rabenau and H. Schulz, J. Less-Common Met. **50**, 155 (1976).
[21] W. Sachse and R. Juza, Z. Anorg. Allg. Chem. **259**, 278 (1949).
[22] J.-P. Doumerc, A. Ammar, A. Wichainchai, M. Pouchard, and P. Hagenmuller, J. Phys. Chem. Solids **48**, 37 (1987).
[23] M. Mansmann, Z. Kristallogr. **122**, 399 (1965).
[24] S. Djurle, Acta Chem. Scand. **12**, 1415 (1958).
[25] A. Janosi, Acta Crystallogr. **17**, 311 (1964).
[26] P. Blaha, K. Schwarz, P. Sorantin, and S.B. Trickey, Comput. Phys. Commun. **59**, 399 (1990).
[27] P. Blaha, K. Schwarz, P. Sorantin, and S.B. Trickey, Computer Code WIEN LAPW, Institüt für Techinische Elektrochemie, TU Wien, Wien, 1988, distributed on a not-for-profit basis.
[28] J.A. Appelbaum and D.R. Hamann, in *Transition Metals*, edited by M.J.G. Lee, J.M Perz, and E. Fawcett (Institute of Physics, Bristol, 1980), p. 111.
[29] P.J. Feibelman, J.A. Appelbaum, and D.R. Hamann, Phys. Rev. B **20**, 1433 (1979).
[30] L. Hedin and B.I. Lundqvist, J. Phys. C **4**, 2064 (1971).
[31] E. Wigner, Phys. Rev. **46**, 1002 (1934).
[32] An additional LCAO calculation, using the Hedin-Lundqvist exchange correlation potential, showed only minor changes of the band structure.
[33] R.M. Dreizler and E.K.U. Gross, *Density Functional Theory* (Springer Verlag, Berlin, 1990).
[34] R.F.W. Bader and P.M. Bedall, J. Chem. Phys. **56**, 3320 (1972).
[35] P.O. Löwdin, J. Chem. Phys. **18**, 365 (1950).